ACS APPLIED MATERIALS & INTERFACES

Research Article

www.acsami.org

Self-healing Nanofiber-Reinforced Polymer Composites. 2. Delamination/Debonding and Adhesive and Cohesive Properties

Min Wook Lee,[†] Seongpil An,[‡] Hong Seok Jo,[‡] Sam S. Yoon,*[,‡] and Alexander L. Yarin*[,†,‡]

[†]Department of Mechanical and Industrial Engineering, University of Illinois at Chicago, 842 West Taylor Street, Chicago, Illinois 60607-7022, United States

[‡]School of Mechanical Engineering, Korea University, Seoul 136-713, Republic of Korea

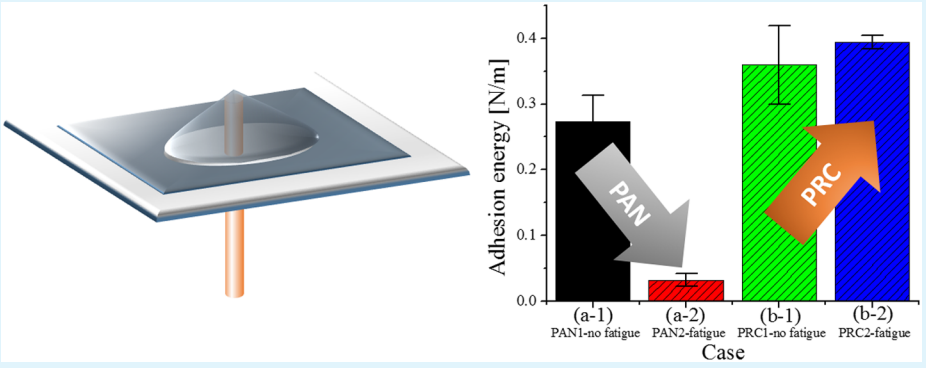

ABSTRACT: The capacity for core−shell nanofiber mats containing healing agents (resin monomer and cure) in their cores to adhere to a substrate was studied using blister testing. After extended periodic bending, the adhesion energy was measured, and the effect of self-healing on the composite's delamination from the substrate was considered. In addition, the cohesion of two layers of the self-healing nanofibers was examined using blister testing and compared to that of ordinary nanofiber mats. The damage inflicted by prolonged periodic bending to the interface of the two nanofiber mats was demonstrated to have self-healed, and the cohesion energy was measured.

KEYWORDS: *self-healing, core−shell nanofibers, electrospinning, composite, delamination*

1. INTRODUCTION

Self-healing in composite materials can repair internal cracks that would otherwise lead to a sudden failure of composite. Recently, the development of self-healing fiber-reinforced composites,[1] concretes,[2] vehicles,[3] mobile phones,[4] and bones[5] has been investigated. These efforts mainly intend to extend the durability and sustainability of engineered materials and the products made from them. Various fatigue elements, such as microcracks and/or delamination surfaces, accumulate in engineered materials that are subjected to periodic loading and unloading. Under certain conditions, the growth of these defects can accelerate to cause catastrophic failure of a macroscopic item, despite the defects' individual sizes being negligibly small for some time. In many cases, these defects occur in the material bulk, invisible to detection and thus evading inspection and repair. Composite materials, whose advanced mechanical properties and light weight lead to wide use in industrial applications, are especially susceptible to these types of defects. Their original inhomogeneity facilitates, in particular, delamination at ply interfaces. Nanofibers with stored healing agents may effectively prevent microcracking and delamination at ply interfaces.[1,6−9]

To study self-healing of delamination at ply interfaces, one must measure the adhesion energy and the effect of released healing agents on this parameter. The adhesion energy of a fiber membrane can be evaluated by the T-peel test,[10] dead-weight test,[11,12] 180° peeling test,[12] and blister test[13,14] in addition to other methods. In the T-peel test, two layers of a long strip of the sample material are adhered under pressure and peeled away from each other. The adhesive strength is a function of the peel force, peel rate, and sample dimensions. Dead-weight testing is used to evaluate the adhesive strength in shear. In this test, a sample is stuck to a target substrate and pulled by a weight connected by a 90° pulley. The weight is provided by a vessel suspended on the pulley and is gradually filled with water during the experiment. The weight of water causing sample detachment from the substrate is referred to as the dead weight transmitted to the adhesive interface. In blister testing, a mechanical shaft pushes an adhesive membrane to induce its delamination from the substrate. The edge effect, inevitable in the T-peel test, can be avoided by employing the approximately conical axisymmetric geometry of the blister test.

In this study, core−shell nanofiber mats with healing materials in the cores were adhered to a substrate, and the

Received: April 22, 2015
Accepted: June 3, 2015
Published: June 3, 2015

DOI: 10.1021/acsami.5b03470
ACS Appl. Mater. Interfaces 2015, 7, 19555−19561

adhesion energy was measured using the blister test following prolonged periodic bending of the samples. In particular, the effect of the self-healing features on the adhesion and delamination was closely studied. For comparison, pristine, damaged, and healed nanofiber mats were studied. Differences in their adhesion and delamination were highlighted by this comparison, permitting elucidation of the composite's self-healing effects.

2. EXPERIMENTAL SECTION

2.1. Materials and Coaxial Electrospinning. The materials used and the coelectrospinning process employed to form nanofiber mats are described in brief in this subsection, with full details given in part 1 of this work [Lee, M. W.; An, S.; Jo, H. S.; Yoon, S. S.; Yarin, A. L. Self-healing Nanofiber-Reinforced Polymer Composites. 1. Tensile Testing and Recovery of Mechanical Properties]. One nanofiber type contained resin monomers (dimethylsiloxane) as a core within a poly(acrylonitrile) (PAN) shell. Another nanofiber type contained cure (dimethylmethyl hydrogen siloxane) in the core and PAN in the shell. Both nanofiber types were coelectrospun simultaneously on a rotating drum to form mutually entangled mats. Nanofiber mats of monolithic PAN nanofibers were also electrospun for comparison.

The above-mentioned nanofiber mats of both types were pressed onto poly(ethylene terephthalate) (PET) substrates with holes in the middle; these fiber–substrate layers were used as samples for blister tests. Some samples were subjected to periodic bending fatigue for 5 h and then rested for 24 h to allow self-healing prior to blister testing. The samples for blister testing were bent with a fixed deflection of 3 mm at a frequency of 1 Hz for 3 h. The 10800 total cycles of repeated bending induced fatigue in the adhered fiber mats. The function shape of the bending deflection applied during the fatigue test is shown in Figure 1.

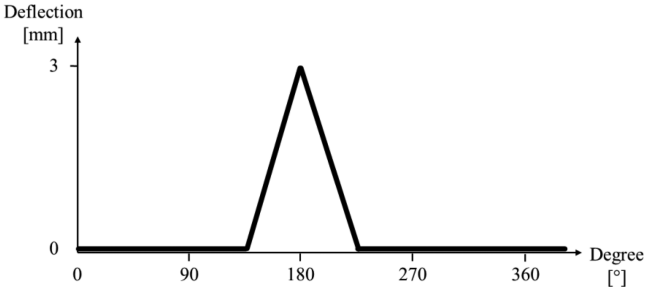

Figure 1. Function shape of the bending deflection applied during the fatigue test. The deflection has been applied using conversion of the rotary motion of a motor (characterized in degrees on the horizontal axis) into the reciprocating motion of a punch acting on a sample.

2.2. Blister Test. The adhesion energies of the prepared nanofiber mats were measured by blister tests.[15,16] The blister test avoids possible edge effects at the delamination and is highly stable/reproducible.[17,18] Most of the previous works on the blister test[15,17,18] dealt with materials whose resistance to bending is associated with the bending stiffness (the moment of the elastic stresses in the cross section), which is felt even at an infinitesimally small bending. The first effort to accommodate the effect of sample stretching important for nonstiff materials involved a crude and unneeded aproximation,[16] as discussed in section 3.3, where a rigorous theoretical foundation for such cases is laid. The mats were cut into pieces with dimensions of 35 mm × 30 mm and placed on a flexible PET plate of 0.73 mm thickness with a 3-mm-diameter hole in the middle. The nanofiber mats were initially pressed to the PET substrates by pressing and rolling a metal roller over the mats, as depicted in Figure 2a. The force applied to the sample through the roller was measured by balance. The metal roller was rolled over the entire sample more than 10 times to guarantee uniform loading and repeatability of the results. This procedure was

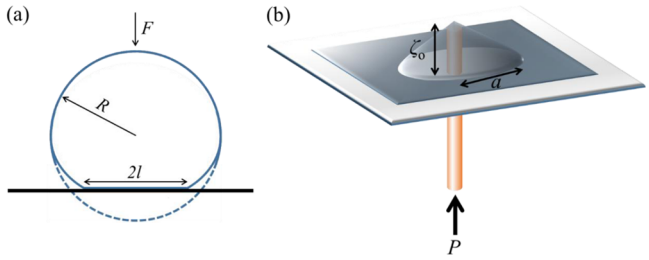

Figure 2. (a) Deformation of an elastic ball pressed to a rigid plane. (b) Schematic of the blister test.

previously used in the literature for similar purposes and is known to enhance the fiber contact and adhesion to the substrate and to remove air entrapped inside the fiber mat.[13,14] The corresponding pressure applied by the roller can be found using the results of ref 19 as

$$l = \left[\frac{3(1-\nu^2)RF}{4E}\right]^{1/3} \quad (1)$$

where l is half the width of the contact area resulting from roller deformation when it is pressed against the rigid surface under the substrate with nanofibers on top, E and ν are the Young's modulus and Poisson's ratio of the metal, respectively, R is the roller radius, and F is the applied force. For a steel roller, E = 200 GPa and ν = 0.3. The roller radius R is equal to 45.5 mm. The hand-pressing force $F \approx 9.2$ kgf = 9.2 kg × 9.81 m/s^2 = 90.25 N. Thus, according to eq 1, $2l$ = 482 μm and the applied pressure $P = F/(w \times 2l)$ (the roller width w = 30.6 mm) to the mat was 6.12 MPa.

A pole with a tip of 0.5 mm in diameter was inserted by an Instron 5942 through the PET substrate's hole and used to delaminate the nanofiber mat from the substrate while the resistance force P was measured (Figure 2b). At the same time, the geometry of the detached nanofiber mat was video-recorded to measure the height ζ_0 and radius a of the resulting blister.

3. RESULTS AND DISCUSSION

3.1. Morphology and Elemental Analysis of the Released Material. Scanning electron microscopy (SEM) images of the pristine nanofiber mats are shown in panels a (PAN) and b [the self-healing PAN–resin–cure (PRC) mat] of Figure 3. Corresponding optical microscopy images of these mats after blister testing are presented in panels c and d of Figure 3, respectively. The PAN nanofibers in Figure 3a are uniform with a cross-sectional fiber diameter of 588 nm. In the pristine self-healing PRC mat in Figure 3b, two different fiber diameters are distinguishable, namely, 1.322 μm and 373 nm. These correspond to the fibers with resin monomer and cure in the cores, respectively. The blister samples were finger-pressed, thus enabling the stored resin monomer to flow out of the cores of broken fibers. Several drops of material released in this manner from the fibers are seen in Figure 3d.

3.2. Blister Testing: Experimental Data. Figures 4 and 5 show the results of blister testing for both PAN and self-healing PRC nanofiber mats. The thicknesses of the PAN and PRC fiber mat were 0.089 and 0.191 mm, respectively. The tests were conducted at different rates, as listed in the figure captions. Figure 4 shows photographs of the mat shapes at different stages of the process.

In Figure 5, the peak force reached in the blister tests strongly depends on the tip motion speed, being lower at 2 mm/min than at 10 mm/min for both materials, whether fatigued or not. The loads recorded in the blister tests of the PRC fiber mats are significantly higher than those recorded in testing the PAN mats. This is caused by the core–shell PRC

DOI: 10.1021/acsami.5b03470
ACS Appl. Mater. Interfaces 2015, 7, 19555–19561

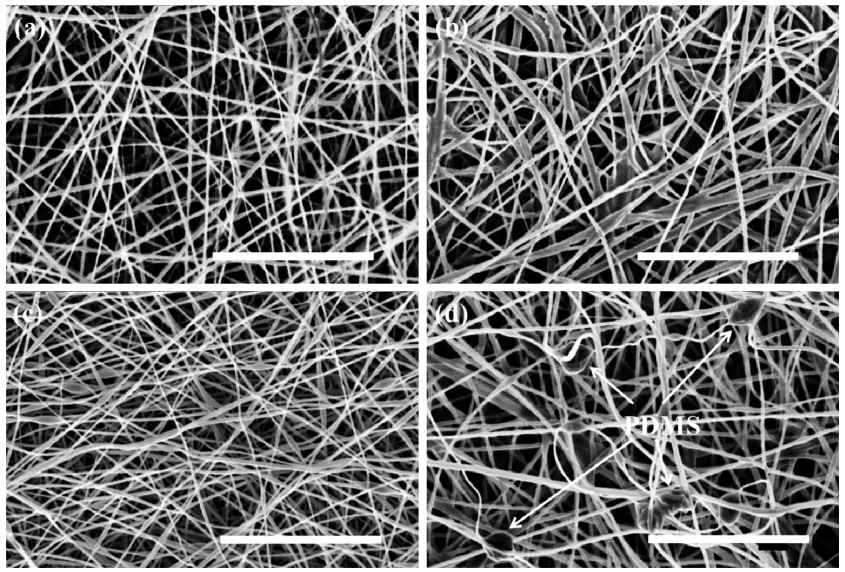

Figure 3. SEM images of pristine fiber mats: (a) PAN nanofiber mat; (b) self-healing PRC nanofiber mat. The same mats after blister testing with released and polymerized PDMS drops visible in several damaged places: (c) PAN nanofiber mat; (d) PRC nanofiber mat. It should be emphasized that the fibrous structure is fully intact even though the metal roller was rolled over the samples more than 10 times. The scale bars are 10 μm (5000× magnification).

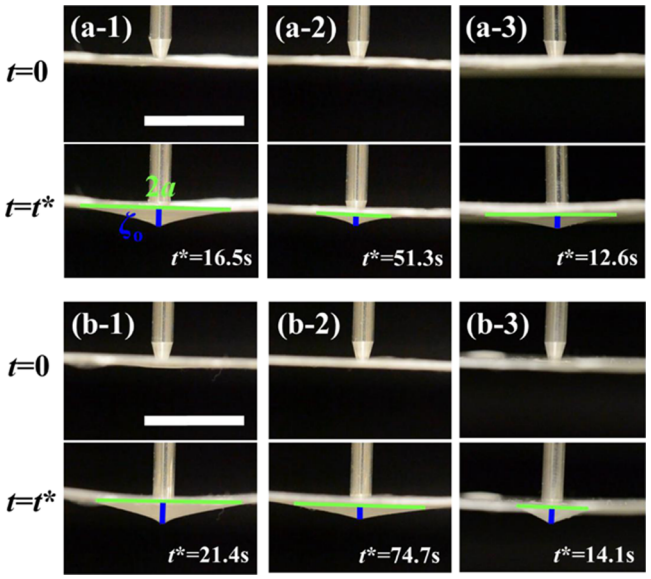

Figure 4. Photographic images of different stages of blister testing. PAN nanofiber mat with tip rates of (a-1) 10 mm/min (pristine mat), (a-2) 2 mm/min (pristine mat), and (a-3) 10 mm/min, where the sample underwent prior periodic bending for 5 h followed by 24 h of rest. PRC sample with tip rates of (b-1) 10 mm/min (pristine mat), (b-2) 2 mm/min (pristine sample), and (b-3) 10 mm/min, where the sample underwent prior periodic bending for 5 h followed by 24 h of rest. Time t = 0 is the beginning of the test, and time t^* is the time of rupture. The values of the rupture time t^* are displayed in the panels.

fibers having already sustained some damage when squeezed between the roller and substrate. As a result, some poly(dimethylsiloxane) (PDMS)−resin monomer and cure have already been released, permitting their polymerization and enhancing of the adhesion between the PRC fibers and substrate.

Figure 5 also depicts the results of blister tests conducted with PAN and PRC mats after 5 h of prior periodic bending. This experiment reveals the effects of prior damage accumulation on the mats' adhesive capacities and evaluates the capability of the PRC fiber mats to prevent delamination. For both the PAN and PRC samples, the peak load achieved in the blister tests after prior periodic bending decreased compared to that for pristine samples (compare curves a-3 and a-1, as well as b-3 and b-1, respectively). This indicates that the prior periodic bending caused significant damage and, in particular, induced fiber delamination from the substrate. Figure 5b shows that the PRC mat did not recover its adhesive strength after periodic bending and a 24-h rest period. This indicates the insufficient release of PDMS−resin monomer and cure at the interface.

It should be emphasized that the abrupt drops of load visible in Figure 5 at later times are typically associated with the beginning of delamination propagation at the blister perimeter similar to a circular self-propagating crack.

The cohesion energy between identical nanofiber mats was also measured using blister tests. For these samples, a PAN or PRC nanofiber mat was fixed to the base PET substrate using dual-sided tape, and then an identical nanofiber mat was placed on top of it and finger-pressed. In Figures 6 and 7, showing the results of these tests, PAN1 and PRC1 denote the corresponding pristine samples, while PAN2 and PRC2 denote the corresponding bending-fatigued samples (with a deflection of 3 mm applied for 3 h with frequency f = 1 Hz; 10800 bending cycles in total). The fatigued samples rested for 24 h after periodic bending for the self-healing PDMS polymerization reaction to proceed. Load−extension curves and photographs taken during these blister tests are depicted in Figures 6 and 7, respectively.

The experimental results are interpreted and discussed in detail in the following subsection.

3.3. Blister Tests: Theory and Evaluation of the Adhesion and Cohesion Energy. The shape of a membrane in a blister test (Figure 2b) is described by the following equation:[20]

DOI: 10.1021/acsami.5b03470
ACS Appl. Mater. Interfaces 2015, 7, 19555−19561

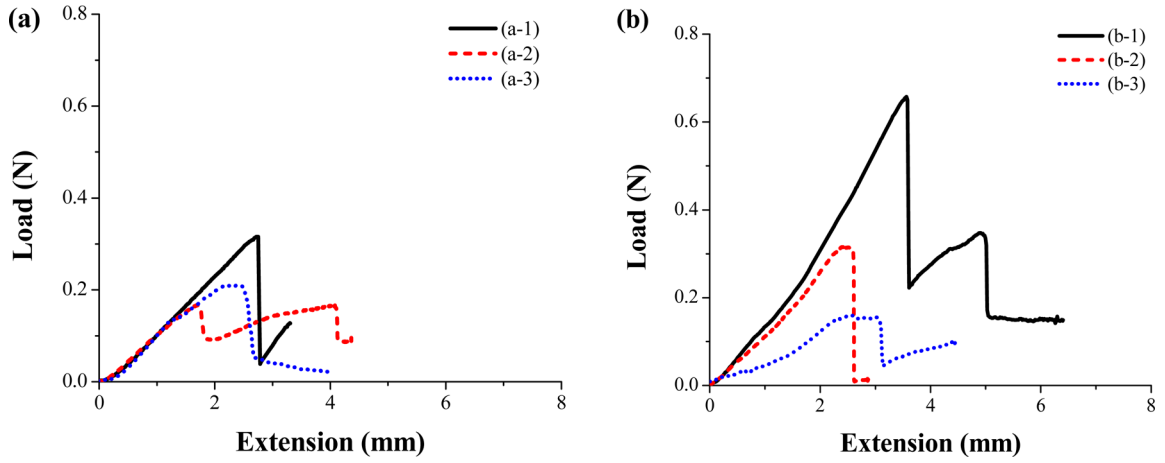

Figure 5. Load–extension curves for blister tests: (a) PAN nanofiber mat; (b) PRC fiber mat. Tip rates: (a/b-1) 10 mm/min, (a/b-2) 2 mm/min, and (a/b-3) 10 mm/min with 5 h of prior periodic bending.

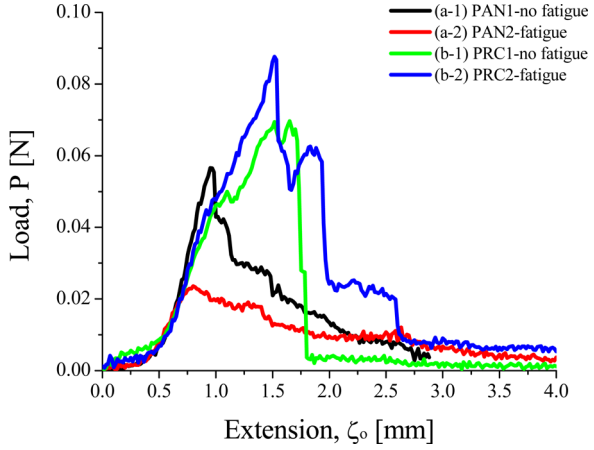

Figure 6. Load–extension curves measured in blister tests.

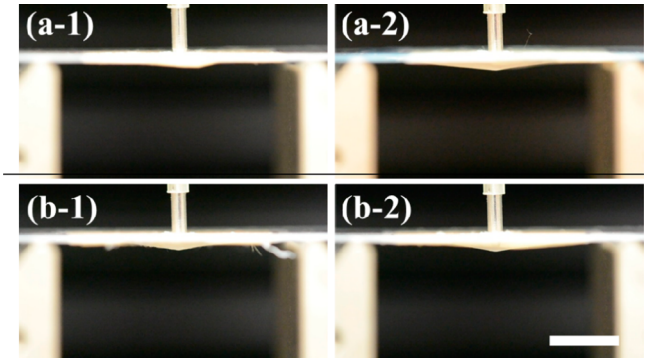

Figure 7. Photographic images of different stages of blister tests: (a-1) PAN without fatigue; (a-2) PAN2 with fatigue; (b-1) PRC without fatigue; (b-2) PRC with fatigue. Scale bar = 10 mm.

$$\frac{Eh^3}{12(1-\nu^2)}\nabla^4\zeta - \nabla\cdot[h\boldsymbol{\sigma}\cdot\nabla\zeta] = K \tag{2}$$

where h is the membrane thickness, E and ν are the Young's modulus and Poisson's ratio of the membrane material, ζ is the elevation of the membrane centerline, $\boldsymbol{\sigma}$ is the stress tensor in the membrane, and K is the distributed vertical force.

The first term on the left in eq 2 is associated with the moment of elastic forces in the membrane's cross section resisting bending, whereas the second term is associated with the resistance due to the elastic force arising as a result of membrane stretching. Accordingly, the first term is linear with the bending amplitude ζ, while the second is nonlinear. When the membrane material is sufficiently stiff, the first term dominates, whereas the second one is negligibly small because the stretching of such materials is small. The resistance to bending in stiff materials is associated with the moment of the elastic stresses in the membrane's cross section. For such stiff materials, the theory of blister tests was developed in ref 14. For soft materials, like the nanofiber mats in this study, the first term in eq 2 is negligibly small, while the main resistance to bending results from the material's resistance to stretching, as expressed in the second term on the left in eq 2. The theory of blister tests proposed in ref 16 began with this point. However, the theory of ref 16 relies on an inappropriate approximation of the blister generatrix as a straight line, which we demonstrate to be incorrect below. Therefore, the results of ref 16 should be considered only as coarse approximations. In the present work, we develop a rigorous theory of blister tests for soft materials.

Consider an axisymmetric blister, using the radial coordinate r on the underlying substrate with the origin at the center of the substrate's hole. Neglecting the first term on the left in eq 2 as negligibly small for soft materials, we transform eq 2 into the following form:

$$\frac{1}{r}\frac{\mathrm{d}}{\mathrm{d}r}\left(h\sigma_{\tau\tau}r\frac{\mathrm{d}\zeta}{\mathrm{d}r}\right) + K = 0 \tag{3}$$

where $\sigma_{\tau\tau}$ is the normal stress component directed along the blister generatrix, which has the unit vector $\boldsymbol{\tau}$.

The stress $\sigma_{\tau\tau}$ arises because of the stretching of the blister generatrix, compared to its initial unstretched shape when it was aligned with the substrate. The corresponding strain is expressed as $\varepsilon_{\tau\tau} = [1 + (\mathrm{d}\zeta/\mathrm{d}r)^2]^{1/2} - 1 \approx (1/2)(\mathrm{d}\zeta/\mathrm{d}r)^2$. Therefore, $\sigma_{\tau\tau} = (E/2)(\mathrm{d}\zeta/\mathrm{d}r)^2$. The pressing force distribution is, as usual in cylindrical cases, $K = (P/2\pi r)\,\delta(r)$, where $\delta(r)$ is the Dirac delta function. Then, eq 3 takes the form of

$$\frac{1}{r}\frac{\mathrm{d}}{\mathrm{d}r}\left[hr\frac{E}{2}\left(\frac{\mathrm{d}\zeta}{\mathrm{d}r}\right)^2\frac{\mathrm{d}\zeta}{\mathrm{d}r}\right] + P\frac{\delta(r)}{2\pi r} = 0 \tag{4}$$

Integrating this equation, subjected to the boundary condition of $\zeta = 0$ at $r = a$, and accounting for the fact that

DOI: 10.1021/acsami.5b03470
ACS Appl. Mater. Interfaces 2015, 7, 19555–19561

for a blister $d\zeta/dr < 0$, we obtained the following expression for the blister generatrix shape:

$$\zeta = \frac{3}{2}\left(\frac{Pa^2}{\pi Eh}\right)^{1/3}\left[1 - \left(\frac{r}{a}\right)^{2/3}\right] \quad (5)$$

This expression for $\zeta(r)$ is nonlinear for any central amplitude of a blister, invalidating the linear assumption made in eq 10 of ref 16, as well as all final results based on that assumption. Notably, these inaccurate results were used for analysis of the results of blister tests in ref 13, rendering these later results inaccurate as well.

The blister height $\zeta_0 = \zeta(r{=}0)$ is found from eq 5 as

$$\zeta_0 = \frac{3}{2}\left(\frac{P}{\pi Eh}\right)^{1/3} a^{2/3} \quad (6)$$

The elastic energy stored in a body, $U_{elastic} = (1/2)\int_V \boldsymbol{\sigma}:\boldsymbol{\varepsilon}\, dV$, where V is the body volume, $\boldsymbol{\varepsilon}$ is the strain tensor, and the colon denotes the scalar product of two second-rank tensors.[20] In the present case,

$$U_{elastic} = \frac{3}{8}\left(\frac{P^4}{\pi Eh}\right)^{1/3} a^{2/3} \quad (7)$$

Blister growth proceeds because of the work of the pushing force P, which is partially stored as internal elastic energy and partially used as a new surface energy associated with the new surface between the nanofiber mat and the underlying substrate when the former delaminates from the latter. This is expressed by the following energy balance:[15]

$$P\, d\zeta_0 = dU_{elastic} + T \times 2\pi a\, da \quad (8)$$

where T is the adhesion energy.

Using eqs 6 and 7, we obtain from eq 8 the following expression for the adhesion energy:

$$T = \frac{3}{8}\left(\frac{1}{\pi^4 Eh}\right)^{1/3}\left(\frac{P}{a}\right)^{4/3} \quad (9)$$

The expression following from ref 16 and used in ref 13 is slightly different:

$$T = \left(\frac{1}{16\pi^4 Eh}\right)^{1/3}\left(\frac{P}{a}\right)^{4/3} \quad (10)$$

We emphasize that eqs 9 and 10 are very similar, only differing in the factor $^3/_8 = 0.375$ versus $16^{-1/3} \approx 0.397$. Equation 9, however, is exact, while eq 10 remains an approximation. Therefore, in the following analysis of the blister test results, we use eq 9.

All of Young's moduli were measured in the independent tensile tests described in the first part of this work [Lee, M. W.; An, S.; Jo, H. S.; Yoon, S. S.; Yarin, A. L. Self-healing Nanofiber-Reinforced Polymer Composites. 1. Tensile Testing and Recovery of Mechanical Properties]. Young's moduli of PAN and the self-healing (PRC) fiber mats are 46.45 and 18.05 MPa, respectively.

The adhesion energy found from experimental data presented in section 3.2 and found using eq 9 is listed in Table 1. The dimensions of the blister ($2a$ and ζ_0) were measured using images similar to those in Figure 4. Notably, at the high tip motion rate of 10 mm/min, the adhesion energy of PRC (experimental curve b-1 in Figure 5) is almost 3 times higher than that of PAN (experimental curve a-1 in Figure 5).

Table 1. Adhesion Energy T

case in Figure 5	extension rate [mm/min]	extension ζ_0 [mm]	a [mm]	P [N]	T [J/m^2 = N/m]
a-1	10	1.81	7.84	0.31578	0.7014
a-2	2	1.01	3.87	0.16691	0.7684
a-3	10	1.19	6.61	0.21218	0.5183
b-1	10	2.17	7.59	0.65736	2.0700
b-2	2	1.66	4.00	0.31542	1.8251
b-3	10	1.54	3.60	0.15276	0.7988

Because of the slight bending of the PET substrate during testing, the extension corresponding to the curves in Figure 5 is slightly higher than that measured from the images in Figure 4. As is seen in Figures 4 and 7, in most of the cases, the PET substrates were not bending at all. Because the samples should also be used in the fatigue tests, the substrates should be flexible to undergo cyclic bending prior to blister tests, which excludes metal or ceramic substrates. Substrate bending happened only in cases a-1 and b-1 in Figure 4 and was practically absent in the other cases. In cases a-1 and b-1, the extension values found from the Instron data (Figure 5) were higher than the corresponding values measured from the images (Figure 4) because of the substrate bending. For that reason, the extension value ζ_0 was determined in such a way that allows one to minimize the inaccuracy associated with substrate bending. As shown in panel a in Figure 8, the elevation at the blister center

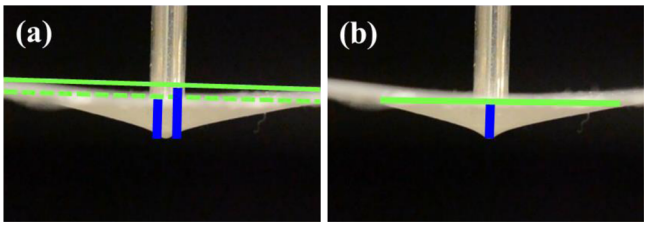

Figure 8. Exclusion of the effect of the substrate bending (if any) on the measured extension value.

(the blue bar) would differ if it would be reckoned from the baseline (corresponding to zero extension: green lines, solid or dashed). To exclude the corresponding error in our measurement where substrate bending was observed, the end of the baseline was set at the beginning of delamination (see panel b in Figure 8). This practically excludes a possible inaccuracy associated with the substrate bending (if any) because the extension is determined only by real delamination of the nanofiber mat from the substrate.

The adhesion energy was found using the measured blister geometry (a and ζ_0) at the highest load P at the rupture moment t^*.

For comparison, the results of blister testing of the nanofiber mats in ref 13 revealed the adhesion energy value of 0.206 ± 0.026 J/m^2, which is significantly lower than those in Table 1. This is in spite of the factor in eq 10, used in refs 13 and16, being higher than the one in eq 9, used in the present work. The difference is due to the fact that ref 13 studied the adhesion of PVDF fibers on cardboard rather than the material set used in the present work.

In the cohesion-related experiments, as shown in Table 2 and Figure 9, PAN and PRC samples behave in diametrically opposed manners after prolonged bending fatigue. A significant decrement in the adhesion energy for the PAN sample

DOI: 10.1021/acsami.5b03470
ACS Appl. Mater. Interfaces 2015, 7, 19555−19561

Table 2. Cohesion Energy *T*

case in Figure 7	ζ_0 [mm]	a [mm]	P [N]	T [J/m^2 = N/m]
a-1	0.95	5.60	0.0566	0.2729
a-2	0.80	9.67	0.0236	0.0321
b-1	1.65	7.13	0.0696	0.3595
b-2	1.52	7.33	0.0876	0.3944

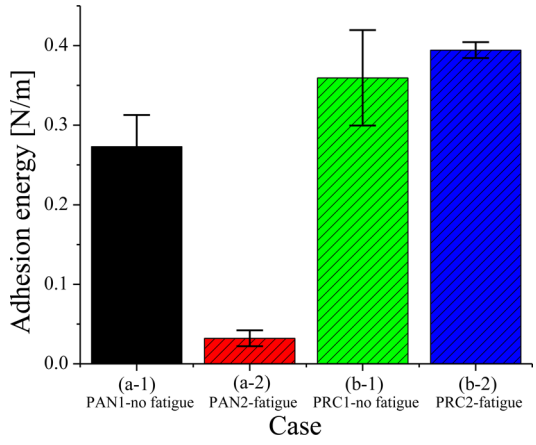

Figure 9. Cohesion energy *T*.

inevitably results from delamination at the nanofiber mat's interface with the PET substrate. The cohesion between the two PAN nanofiber mats has also been weakened by prolonged repeated bending, with no way to recover from such damage. On the contrary, the PRC samples containing PDMS resin monomer and cure display an increase of about 10% in the measured cohesion energy. This implies that the healing agents were released from the nanofiber cores and polymerized, thus restoring and reinforcing the cohesion at the damaged interface.

4. CONCLUSIONS

After prolonged periodic bending fatigue, self-healing composite nanofiber mats revealed a restored, and even increased by 10%, cohesion energy at the interface between two layers. This resulted from the release of resin monomers and cure from the nanofiber cores, which permitted a PDMS polymerization reaction. However, the adhesion energy of self-healing nanofiber mats to a solid flexible substrate was not restored in this way, even though the adhesion energy in the pristine samples exceeded the cohesion energy.

Periodic bending fatigue is characteristic of the joint area between an airplane wing and the plane's body. The repeated up-and-down motions during flights and landings result in mechanical fatigue in the joint, causing weakening. The bending is repeated on a time scale of 10−20 years of service; the accumulated delamination damage can result in an almost instantaneous catastrophic event. Self-healing nanofiber mats may provide self-sustained material cohesion in such areas.

AUTHOR INFORMATION

Corresponding Authors

*E-mail: ayarin@uic.edu. Phone: (312) 996-3472. Fax: (312) 413-0447.

*E-mail: skyoon@korea.ac.kr. Phone: +82-2-3290-3376. Fax: +82-2-926-9290.

Notes

The authors declare no competing financial interest.

ACKNOWLEDGMENTS

This work was primarily supported by the International Collaboration Program funded by the Agency for Defense Development. This work was partially supported by ISTDP (10045221), GFHIM (NRF-2013M3A6B1078879), and NRF-2013R1A2A2A05005589.

REFERENCES

(1) Wu, X.-F.; Rahman, A.; Zhou, Z.; Pelot, D. D.; Sinha-Ray, S.; Chen, B.; Payne, S.; Yarin, A. L. Electrospinning Core−Shell Nanofibers for Interfacial Toughening and Self-Healing of Carbon-Fiber/Epoxy Composites. *J. Appl. Polym. Sci.* **2012**, *129* (3), 1383−1393.

(2) Song, Y.-K.; Jo, Y.-H.; Lim, Y.-J.; Cho, S.-Y.; Yu, H.-C.; Ryu, B.-C.; Lee, S.-I.; Chung, C.-M. Sunlight-Induced Self-Healing of a Microcapsule-Type Protective Coating. *ACS Appl. Mater. Interfaces* **2013**, *5* (4), 1378−1384.

(3) Greig, D. Self-healing car paint uses sunlight to repair scrapes. 2009, http://www.gizmag.com/self-healing-car-paint/11254/.

(4) Davies, A. LG Demonstrates Self-Healing G Flex Curved Phone. 2014, http://www.tomshardware.com/news/lg-g-flex-healing-phone-preview,25805.html.

(5) Norris, C. J.; Meadway, G. J.; O'Sullivan, M. J.; Bond, I. P.; Trask, R. S. Self-Healing Fibre Reinforced Composites via a Bioinspired Vasculature. *Adv. Funct. Mater.* **2011**, *21* (19), 3624−3633.

(6) Lee, M. W.; An, S.; Lee, C.; Liou, M.; Yarin, A. L.; Yoon, S. S. Self-Healing Transparent Core−Shell Nanofiber Coatings for Anti-Corrosive Protection. *J. Mater. Chem. A* **2014**, *2* (19), 7045−7053.

(7) Lee, M. W.; An, S.; Lee, C.; Liou, M.; Yarin, A. L.; Yoon, S. S. Hybrid Self-Healing Matrix Using Core−Shell Nanofibers and Capsuleless Microdroplets. *ACS Appl. Mater. Interfaces* **2014**, *6*, 10461−10468.

(8) Sinha-Ray, S.; Pelot, D. D.; Zhou, Z. P.; Rahman, A.; Wub, X.-F.; Yarin, A. L. Encapsulation of Self-Healing Materials by Coelectrospinning, Emulsion Electrospinning, Solution Blowing and Intercalation. *J. Mater. Chem.* **2012**, *22*, 9138−9146.

(9) Wu, X.-F.; Yarin, A. L. Recent Progress in Interfacial Toughening and Damage Self-Healing of Polymer Composites Based on Electrospun and Solution-Blown Nanofibers: An Overview. *J. Appl. Polym. Sci.* **2013**, *129*, 2225−2237.

(10) Ballarin, F. M.; Blackledge, T. A.; Davis, N. L. C.; Frontini, P. M.; Abraham, G. A.; Wong, S.-C. Effect of Topology on the Adhesive Forces Between Electrospun Polymer Fibers Using a T-peel Test. *Polym. Eng. Sci.* **2013**, *53*, 2219−2227.

(11) Najem, J. F.; Wong, S.-C.; Ji, G. Shear Adhesion Strength of Aligned Electrospun Nanofibers. *Langmuir* **2014**, *30*, 10410−10418.

(12) Sett, S.; Lee, M. W.; Weith, M.; Pourdeyhimi, B.; Yarin, A. L. Biodegradable and Biocompatible Soy Protein/Polymer/Adhesive Sticky Nano-Textured Interfacial Membranes for Prevention of Esca Fungi Invasion into Pruning Cuts and Wounds of Vines. *J. Mater. Chem. B* **2015**, *3*, 2147−2162.

(13) Na, H.; Chen, P.; Wan, K.-T.; Wong, S.-C.; Li, Q.; Ma, Z. Measurement of Adhesion Work of Electrospun Polymer Membrane by Shaft-Loaded Blister Test. *Langmuir* **2012**, *28*, 6677−6683.

(14) Wong, S.-C.; Na, H.; Chen, P. Measurement of Adhesion Energy of Electrospun Polymer Membranes Using a Shaft-loaded Blister Test. *13th Int. Conf. Fract.* **2013**, 1−7.

(15) Malyshev, B. M.; Salganik, R. L. The Strength of Adhesive Joints Using the Theory of Cracks. *Int. J. Fract. Mech.* **1965**, *1* (2), 114−128.

(16) Wan, K.-T.; Mai, Y.-W. Fracture Mechanics of a Shaft-Loaded Blister of Thin Flexible Membrane on Rigid Substrate. *Int. J. Fract.* **1995**, *74*, 181−197.

(17) Obreimoff, J. W. The Splitting Strength of Mica. *Proc. R. Soc. London, A* **1930**, *127*, 290−297.

(18) Hutchinson, J. W.; Suo, Z. Mixed Mode Cracking in Layered Materilas. *Adv. Appl. Mech.* **1992**, *29*, 63−191.

DOI: 10.1021/acsami.5b03470
ACS Appl. Mater. Interfaces 2015, 7, 19555−19561

(19) Derjaguin, B. V.; Muller, V. M.; Toporov, Y. P. Effect of Contact Deformations on the Adhesion of Particles. *J. Colloid Interface Sci.* **1975**, *53* (2), 314−326.
(20) Landau, L. D.; Lifshitz, E. M. *Theory of Elasticity*; Pergamon Press: Oxford, U.K., 1970.

DOI: 10.1021/acsami.5b03470
ACS Appl. Mater. Interfaces 2015, 7, 19555−19561